Journal of Pharmaceutical Sciences 109 (2020) 2798-2811

Contents lists available at ScienceDirect

Journal of Pharmaceutical Sciences

journal homepage: www.jpharmsci.org

Pharmaceutics, Drug Delivery and Pharmaceutical Technology

An Imaging Toolkit for Physical Characterization of Long-Acting Pharmaceutical Implants

Daniel Skomski [a, *], Zhen Liu [b], Yongchao Su [b], Christopher T. John [b], Amy Doty [c], Seth P. Forster [b], Ryan Teller [b], Stephanie E. Barrett [a], Wei Xu [b]

[a] Merck & Co., Inc., Rahway, New Jersey 07065
[b] Merck & Co., Inc., West Point, Pennsylvania 19486
[c] Merck & Co., Inc., Boston, Massachusetts 02115

ARTICLE INFO

Article history:
Received 19 March 2020
Revised 26 May 2020
Accepted 27 May 2020
Available online 11 June 2020

Keywords:
Implant
LAP
Long-acting
Imaging
Microscopy
Polymer
Dispersion
X-ray CT

ABSTRACT

In pharmaceutical development alternative drug delivery modalities are being increasingly employed. One example is an implant, which achieves gradual drug release in patients over a period of many months or years. Due to the complexity of these long-acting formulations, advanced physical characterization methods are desirable as screening tools during protracted formulation development. Imaging methods are of particular interest due to their ability to interrogate the structure and composition of implants spatially across multiple length scales (macro, micro, nano). In this work, spatiochemical imaging is shown to interrogate many crucial drug product attributes of solid implants: overall implant structure, drug distribution, micro-domain size and orientation, agglomeration, porosity and defects, drug/excipient interface, dissolution process, and release mechanism. Imaging methods facilitate a detailed understanding of the process/structure correlation to inform on formulation selection, process parameter optimization, and batch consistency. Numerous case studies of implant applications with imaging are discussed. Methods utilized are X-ray computed tomography (XRCT), scanning electron microscopy (SEM), energy-dispersive X-ray spectroscopy (EDS) imaging, and Raman microscopy. The imaging data is complemented with solid-state nuclear magnetic resonance (ssNMR). Altogether, these examples demonstrate that complementary imaging methods are highly effective for analyzing complex and novel pharmaceutical modalities such as solid implants.

Introduction

In the pharmaceutical industry there is a strong drive towards alternate drug delivery systems.[1,2] Long-acting formulations are intended to improve patients' adherence to their medication and prevent therapeutic failure.[3-6] Pharmaceutical implants are of interest because they gradually release drug in patients over a period of many months or years.[3] While implants afford extended drug release, they are complex formulations that require protracted development timelines. Sophisticated physical characterization tools are needed to better understand the technical considerations that underpin the workings of these formulations.

Imaging methods hold promise for materials physical characterization of long-acting polymeric implants. In the pharmaceutical space, imaging has been employed in an *in-vivo* and biological setting[7,8] and has also found ample applications in formulation development of tablets, capsules, coatings, and other materials by various methods.[9-11] In this work the applications of numerous imaging techniques to long-acting polymeric implants are discussed for interrogating material aspects of formulations. The implants are composed of polymer as well as a small molecule or peptide drug. The techniques discussed are X-ray computed tomography (XRCT), scanning electron microscopy (SEM), energy-dispersive X-ray spectroscopy scanning electron microscopy (EDS-SEM), and Raman microscopy. Solid-state nuclear magnetic resonance (ssNMR) is also leveraged.

In the context of long-acting implants, many studies of have been conducted which have emphasized *in-vivo* and *in-vitro* imaging applications.[12-15] On the other hand, the exploration of materials imaging technologies to interrogate the influence of manufacturing processes on solid implants is less well-treaded territory. For example, in prior comprehensive summaries of the effect of manufacturing processes on material attributes of polymerics fabricated by hot melt extrusion (HME)[16] materials imaging was not a major point of emphasis. Thus, material characterization technologies for solid polymeric implants would benefit from

* Corresponding author.
E-mail address: dskomski@indiana.edu (D. Skomski).

https://doi.org/10.1016/j.xphs.2020.05.031
0022-3549/

further method development and application to achieve more widespread industrial adoption. To the best of our knowledge, the comprehensive study of the influence of implant manufacturing processes on a broad range of formulation material attributes for solid subcutaneous implants and their effect on performance and quality control, studied at multiple spatial length scales (macro/micro/nano) using multiple advanced imaging techniques, provides additional insights.

Imaging for materials characterization affords numerous benefits towards pharmaceutical development of polymeric implants which are discussed in detail. Broadly speaking, imaging can be utilized to assist in selection of the lead formulation design and preferred manufacturing process by evaluating the structure and spatial composition of the formulations that are produced. Imaging can aid in process parameter selection and optimization by interrogating the impact of the operating conditions on the resultant formulation. Imaging can also be used for quality control to ensure that the formulations are structurally uniform and that different batches are produced with consistent attributes. Furthermore, imaging tools can be used to aid in an understanding of the drug release mechanism and confirm that the drug releases in an expected way.

Materials and Methods

X-Ray Computed Tomography (XRCT)

XRCT was performed on a Xradia Versa XRM-500. The samples were imaged as-received without additional sample modification. The image acquisition and reconstruction software utilized was VersaXRM and XMReconstructor, respectively (software revision July 10, 3679.13921).

XRCT is utilized for 3D imaging. Whereas many other microscopic methods primarily investigate the surface region of materials, the X-rays penetrate the solid organic drug product formulation and enable the reconstruction of a full three-dimensional representation of the entire object. In so doing, it is possible to examine the interior of drug products in a non-destructive manner. XRCT generates intrinsic contrast differences between some features in a formulation, which is dependent on factors including the physical density of the material and the elemental atomic number of the substituents. For example, in a typical XRCT grayscale scan of a solid drug product, it is common that low-density regions like air pockets will appear with low intensity in the images (dark regions), whereas high-density regions of metal excipients appear with high intensity (bright regions). In this study, XRCT yielded contrast differences between some of the formulation components. For example, crystalline small-molecule drug domains appeared with higher intensity (brighter) than semi-crystalline polymer domains. Regions of metal excipients such as barium sulfate appeared with higher intensity (brighter) than either the crystalline API or the semi-crystalline/amorphous polymer regions.

For solid drug product formulations XRCT is used to assess the global uniformity (porosity, deformities, *etc.*) and microstructural features (domain size, shape, orientation, *etc.*). Another benefit is that XRCT can be employed for characterization at multiple spatial length scales. At a low magnification setting, the whole implant drug product radial cross-section is imaged (2 mm diameter) and macro-scale uniformity is assessed (pixel size 2.2 μm). At a high magnification setting, higher-resolution images are acquired albeit of a smaller region (650 μm diameter volume; pixel size 700 nm).

A major limitation of XRCT is that the method does not possess a high degree of chemical differentiation (unlike chemical mapping which is also discussed in this work). Therefore, some substituent components of a formulation cannot be distinguished with XRCT. Further, due to its spatial resolution limitation, micro-XRCT is not capable of observing molecular-level structures and generally resolved only micro-agglomerate particle structures in these studies.

Data representation and data analysis was performed with ORS Dragonfly Pro v.2.0.0.0. For image segmentation of pertinent features from X-ray CT images, different image analysis methods were employed, including threshold-based segmentation and the Otsu method.[17] In Fig. 2, porosity was computed from XRCT of four samples using thresholding-based image segmentation. The measurement carries an error bar for porosity of approximately ±0.5% due to the limitations inherent to a thresholding segmentation approach, though this analysis proved adequate and did not appreciably impact the conclusions of this study as the porosity differences cited in Fig. 2 varied greatly between the samples tested. Further, the porosity cited captures macro- and micro-porosity only (not nano-porosity due to the resolution limitation of XRCT).

Scanning Electron Microscopy (SEM) and Energy Dispersive X-Ray Spectroscopy (EDS)

Due to its widespread utility, SEM has many applications. In this work SEM is used to assess the local nanostructure of implants. With SEM we can analyze the structure of materials with a much higher spatial resolution than is possible with XRCT. For example, in this study SEM was able to resolve single drug particles inside the implant solid dispersion matrix (whereas XRCT could only resolve micro-agglomerate clusters composed of multiple drug particles). SEM examines regions at the surface of a material, but can also be combined with destructive methods to dissect samples in order to obtain structural information on the interior of the implants.

A further benefit is that SEM is paired with EDS for elemental mapping to examine the local elemental distribution of substituent components in the formulation. In this manner, the micro-distribution of species can be more reliably determined; *e.g.*, halogen-containing APIs and metal-containing excipients yield distinct spectral signatures that can be mapped. A full review of SEM is beyond the scope of this work and readers are encouraged to reference a range of publications on this technique and its pharmaceutical applications in the literature.

Samples were cryotomed using a metallic blade into thin sections and then fixed to an aluminum stub using double-sided carbon adhesive tape. Metallic coating of the samples was not employed. Environmental scanning electron microscopy (ESEM) was performed for implant imaging with a FEI Quanta 250 FEG. Scanning parameters utilized include 20 kV, ~150 μA emission current, large field detector, FEI Quanta 250 FEG beam spot size setting #2, and 10.0 mm working distance. A controlled 0.75 Torr water pressure was introduced into the chamber to minimize charging of the sample during acquisition. Elemental analysis by EDS was performed using an Oxford Instruments Energy Dispersive X-ray (EDX) detector and an acquisition time of 2−5 min. Spectra were collected for regions of interest and processed using the Oxford Instruments INCA software suite, smoothing step, elimination of Si escape peaks, Gaussian deconvolution, and the ZAF quantitation method. For EDS mapping, to achieve adequate signal, the water pressure inside the chamber was reduced to 0.3 Torr. The EDS map was collected over a 350 μm region at a pixel mapping resolution of 1024 × 704.

Raman Microscopy

Raman imaging is a chemical imaging method for quantitative analysis of multi-component systems. It has been shown to possess utility for the analysis of oral, inhaled, and other pharmaceutical drug products.[18] A primary benefit is that Raman is chemically sensitive

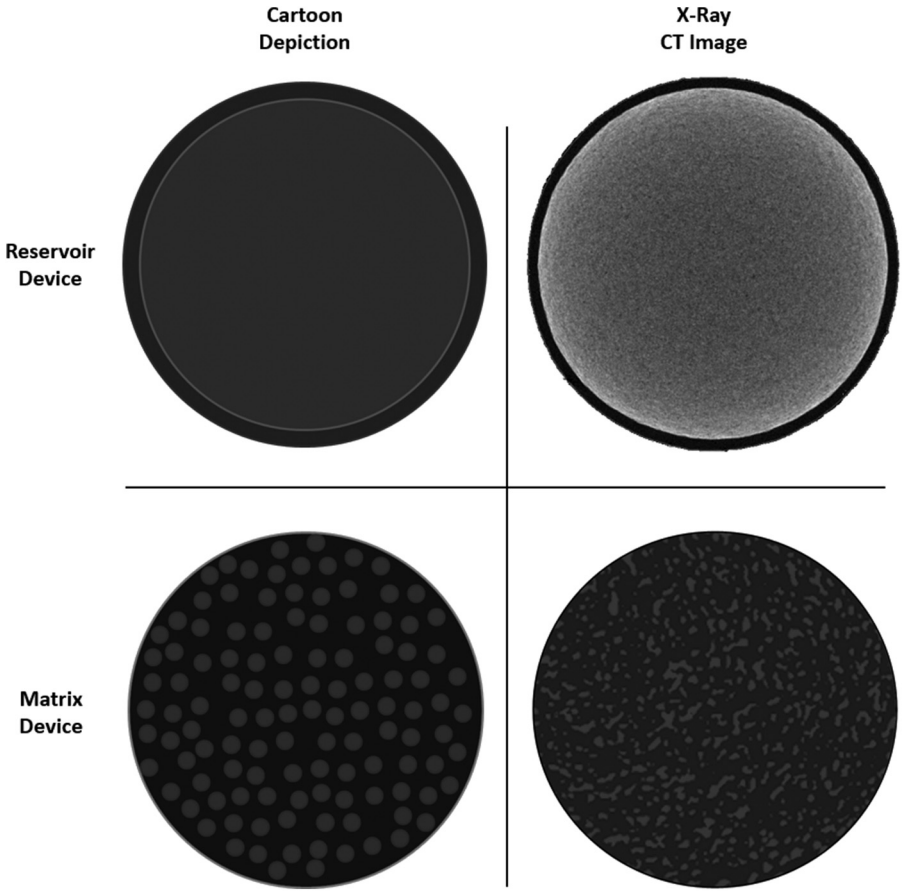

Fig. 1. Two implant designs comparing the intended design to the actual structure evaluated by X-ray CT imaging. Top row: Reservoir implant composed of a drug-rich core and a drug release rate-controlling outer polymer layer (image dimension: 2 μm). Bottom row: Matrix implant composed of a solid-dispersion of drug in a polymer matrix (image dimension: 0.6 μm).

(unlike XRCT). Further, Raman is sensitive to different moieties of organic pharmaceutical materials which elemental mapping cannot distinguish. Thus, the tool can be used to spatiochemically map complex pharmaceutical drug product compositions.

Raman microscopy was conducted on a Renishaw Invia Qontor microscope with a 785 nm line-focused laser, a 50× objective, an acquisition step size of 5 μm, and a mapped area size of $500 \times 500\ \mu m^2$. Reference standards were prepared of the API, the polymer (ethylene vinyl acetate), and barium sulfate ($BaSO_4$), which demonstrated effective spectral separation between the components.

Sample Fabrication General Information

Most of the implant samples discussed in this work were prepared using a hot melt extrusion (HME) process. For the HME samples the API and milled polymer were preblended and hot-melt extruded to form rods of approximately 2 mm in diameter. A couple of implants discussed were prepared by a solvent casting method, as outlined in the next section and explicitly noted in the manuscript. One implant was made by a small-scale tubing process by melting the polymer inside a hollow tube in order for it to attain its desired cylindrical rod shape.

The active pharmaceutical ingredient (API) primarily utilized in this study is a highly-soluble BCS class 1 compound. The API is highly stable in the crystalline form. Due to the high solubility of the API, it would be completely dissolved in the pure powder form in a matter of seconds or minutes.

Sample Fabrication by Hot Melt Extrusion (HME)

Micronized polymer and API were blended with a Turbula T2F mixer at various ratios. Two screw configurations were used, both predominately consisting of conveying elements with different mixing sections. The less aggressive screw design ("HME low shear") contained a mixing section consisting of conveying, kneading elements each 15 mm in length, with offset angles of 30°, 60°, and 60°. The more aggressive screw design ("HME high shear") included additional mixing segments after the mixing section used in the less aggressive design: conveying, kneading elements each 15 mm in length, with an offset angle of 90°. For both extrusion setups, the strands were then air-cooled and pelletized to form micropellets. The pellets were then extruded with a ½" American Kuhne single screw extruder to form a 2 mm diameter filament.

A complementary spectroscopic method, solid-state nuclear magnetic resonance (ssNMR), was used to confirm formation of a phase-separated system.

Sample Fabrication by Solvent Casting

Miniature cylindrical implants were prepared using solvent-casting methods analogous to those previously described by other authors.[19-21] Polymer (PCL, PLA, or PLGA) was dissolved in a volume of organic solvent (*e.g.*, acetone, dichloromethane) to form a solution of appropriate viscosity to allow for extrusion and solid implant formation. API was added to the polymer solution as a solid or in solution with a second organic solvent (*e.g.*, methanol). Depending on the properties of API and solvents used, this resulted in either a suspension of API in the polymer solution, a solution of

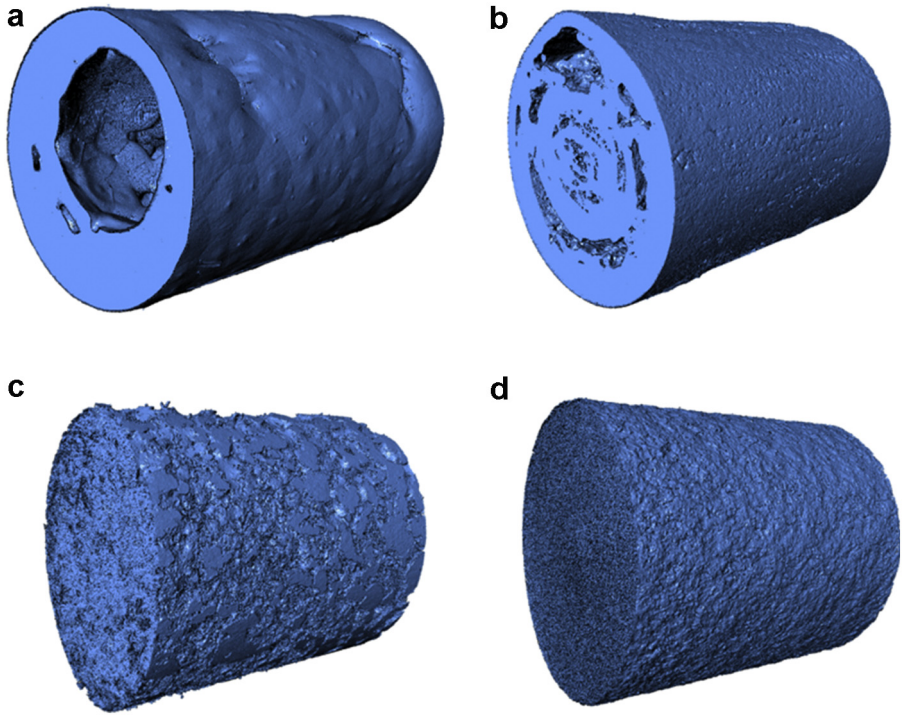

Fig. 2. X-ray CT 3D reconstructions of matrix implants produced by four different implant fabrication methods. (a) Mixed solvent-cast method (31% porosity). (b) Single solvent-cast method (18% porosity). (c) Tubing process and melting the polymer inside the tube (7% porosity). (d) Good manufacturing process (GMP)-scale hot melt extrusion setup with optimized process conditions («1% porosity). The spatial resolution pixel size of the XRCT data is 2.2 μm. Each cylindrical implant has a cylindrical diameter of ca. 2 mm.

API and polymer in a single-solvent system, or a solution of API and polymer in a mixed-solvent system. This mixture was extruded into silicone tubing (inner diameter = 1.6 mm) using a needle and syringe at a flow rate of approximately 0.1 mL/min, until the tubing was completely full. The ends of the tubing were sealed, and the system was then dried under vacuum at room temperature for 48 h (The tubing is semi-permeable to gas and the solvent escapes through the tubing. Also, the seals at the end of the tube are not entirely impenetrable to the air while drying.) Once dry, the tubing was removed and the resulting rigid miniature implant was cut into segments of desired length for analysis.

Solid-State NMR Spectroscopy

^{13}C cross polarization (CP) magic angle spinning (MAS) spectra are acquired at a 400 MHz Bruker Advance III HD spectrometer in the Pharmaceutical NMR lab of Preclinical Development at MRL (Merck & Co., Inc., West Point, PA, USA). A 1.2 ms CP contact time, 50 s recycle delay, 83 kHz SPINAL decoupling are utilized. All experiments are carried out using a Bruker 4 mm HFX MAS probe in double-resonance mode tuned to ^{1}H and ^{13}C, at 12 kHz MAS spinning and at 294 K. Typical pulse powers are 3 us and 4 us for ^{1}H and ^{13}C, respectively. The ^{13}C chemical shifts are referenced externally by using tetramethylsilane (TMS). All spectra are processed in TopSpin.

Results and Discussion

Macro-Scale Imaging for Formulation Design and Manufacturing Process Selection

In the late stages of pharmaceutical drug discovery and early stages of implant development, when the aim is to design

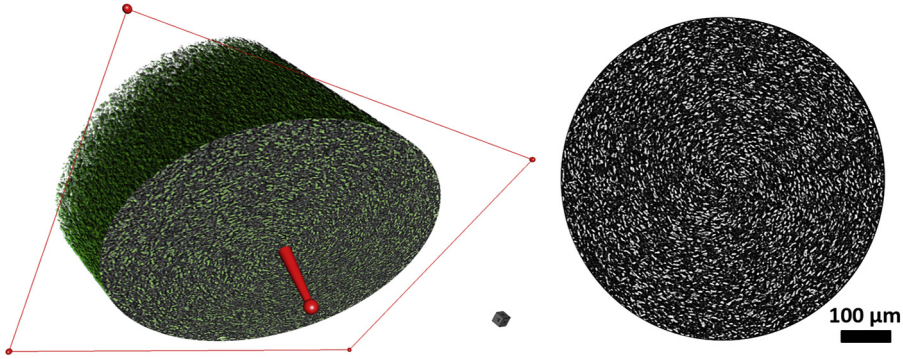

Fig. 3. X-ray CT of a solid-dispersion matrix implant. (a) A 650 μm volume of a virtually dissected implant, demonstrating how it is possible to "slice" implant samples by software analysis and examine the micro-structure on the interior of the implant non-destructively. (b) 2D cross-sectional image. The crystalline drug domains appear as white dots and the polymer matrix is shown by the darker color.

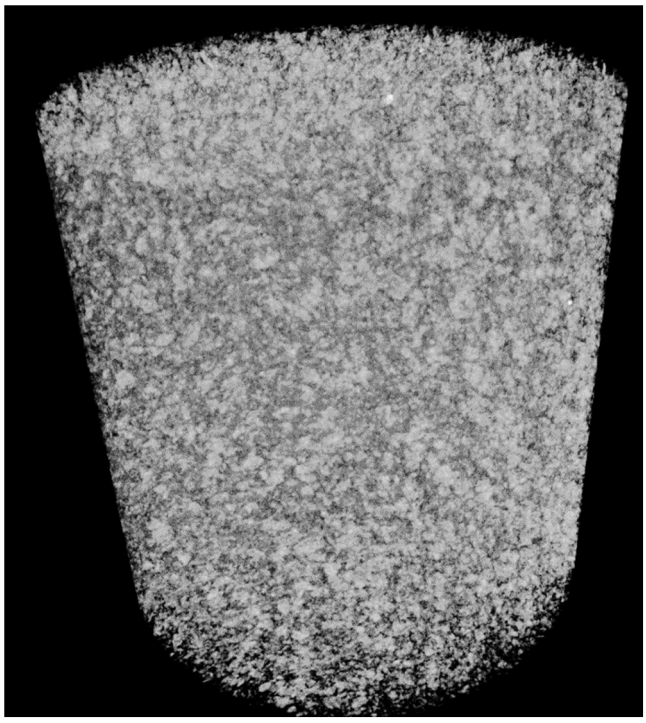

Fig. 4. X-ray CT reconstruction of a 650 μm volume inside a matrix solid-dispersion implant showing the drug domain structure in 3D. The drug domains are shown in white. The polymer was digitally omitted for clarity. The drug loading by weight is 10%.

prototype formulations to achieve long-acting release, we demonstrate that imaging can be applied to aid in the selection of the formulation design for solid polymeric implants by evaluating the feasibility of the manufacture of a particular design as well as the preferred manufacturing method.

In Fig. 1 a comparison is shown of two implant formulation designs along with corresponding X-ray CT images. One example is a reservoir system composed of a core enriched with drug and a polymeric outer shell. This design is reliant upon diffusion of drug through the shell which acts as the rate-limiting step towards gradual release over time. The image confirms that that the core and shell were fabricated and that the targeted shell thickness was achieved (in this case, 60 μm). The second example is a matrix design which is composed of a solid dispersion of drug particles inside a polymer matrix. The image shows that drug domains are uniformly dispersed in the formulation. The two formulation designs have fundamentally a completely different mechanism of release. These examples illustrate that 3D imaging can be used to confirm that the physical structures of fabricated implants conform to their intended designs. The remainder of this work is focused principally on implants of the solid-dispersion matrix design.

With a formulation design identified and confirmed, Fig. 2 demonstrates the utility of imaging to compare different manufacturing methods. The formulations are solid-dispersion matrix implants composed of drug and polymer, but were fabricated using different manufacturing techniques. Imaging is used to assess the overall structural uniformity of the resultant formulations. Specifically, through image analysis segmentation of regions of low physical density (air cavities) from regions of higher physical density (drug/polymer material), the total macro- and micro-porosity in the implant is computed quantitatively (details of the porosity computation are provided in the XRCT methods section). This methodology affords a more benign assessment of internal air pockets compared to, *e.g.*, mercury porosimetry. A high porosity decreases the absolute quantity of drug and polymer in the solid implant and, if pore formation is poorly controlled and unintentional, holds the potential to increase variabilities between batches. It is also understood that, for a solid-dispersion matrix implant, the porosity can have a significant impact on the drug release rate by altering the available surface area for dissolution.

The first set of examples of implants in Fig. 2a and b were manufactured with solvent casting using a mixed solvent and single solvent system, respectively. Solvent casting is a simple and low-cost method that can be applied to understand the suitability of a particular drug for an implant formulation. Imaging reveals that the formulation that was produced from a mixed solvent system (Fig. 2a) contained very large air cavities. The porosity of the implant in Fig. 2a is 31%. On the other hand, the formulation produced from a single solvent system (Fig. 2b) was found to contain a reduced propensity towards air pockets (18% total porosity). A single-solvent method thus was identified to hold promise for preliminary screening efforts of the implant formulations. Another case is presented in Fig. 2c of an implant fabricated from a small-scale tubing process by melting polymer inside a hollow tube to attain the desired cylindrical rod shape. Imaging confirms that the resultant formulation does not possess major macro-scale defects. Furthermore, the volume consumed by air pockets in this formulation is substantially reduced (7% total porosity). However, this process still introduces some imperfections which are unrepresentative of commercial-scale

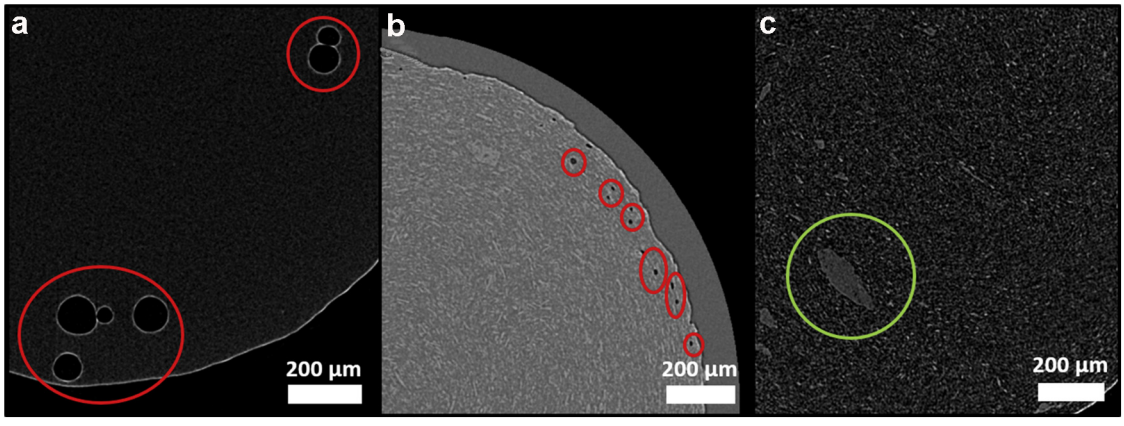

Fig. 5. XRCT 2D cross-sections showing defects that may be observed in implants fabricated under un-optimized process conditions. (a,b) Air pockets of varying sizes (red circles). (c) Drug agglomerates (green circle).

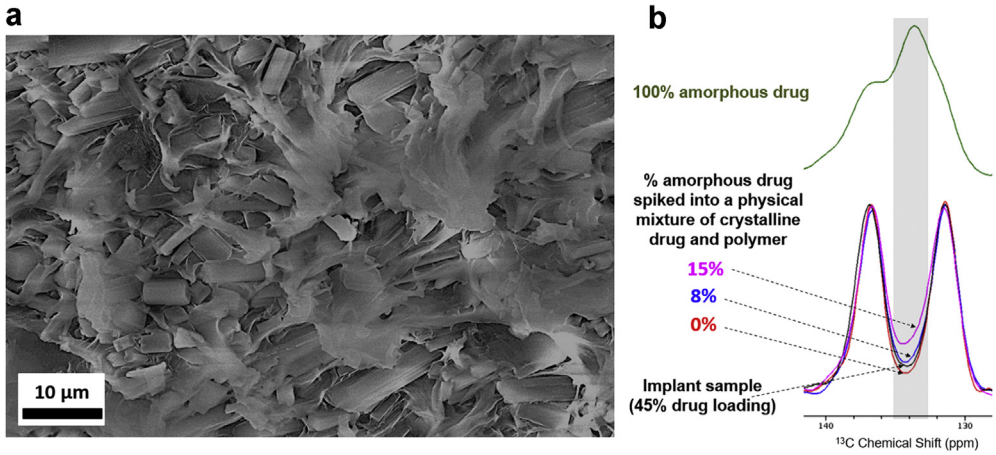

Fig. 6. (a) SEM secondary electron image of a cross-section of an implant formulation. (b) ^{13}C CP-MAS NMR spectra indicating effective phase separation between drug and polymer in the implant, as suggested by the imaging data.

extrusions. Lastly, the sample in Fig. 2d is an implant generated from a good manufacturing practice (GMP) HME instrument utilizing optimized conditions. Imaging reveals that the resultant implants possess a high degree of structural uniformity («1% total porosity). The results demonstrate that XRCT is an effective first-pass assessment of general formulation uniformity during the implant formulation screening phase. The macro-uniformity has a direct impact on release performance and product quality. In our experience, for the solid dispersion implants studied, formulations possessing large internal air cavities exhibited a faster release rate due the increased surface area for dissolution. Additionally, it can be challenging to control air pocket formation reliably during manufacturing, and therefore a more uniform implant is preferred from the standpoint of achieving long-term formulation quality control and robustness.

Formulation Micro-Structural Uniformity and Batch Consistency

In the prior section imaging was applied to understand different implant designs and manufacturing methods. Having examined the macro-scale structure of the formulations, the objective now is to understand the micro- and nano-scale structure of these solid dispersion matrix implant formulations.

Micro-Scale Uniformity

Imaging methods enable evaluations of the micro-scale structure of implants, which we demonstrate can be an important factor impacting the drug release profiles (as will be further discussed in subsequent sections). Micro-imaging is used to confirm a spatially uniform distribution of drug and excipients in the formulation. In addition, other defects can be evaluated, such as the extent of drug agglomeration and presence of small micron-sized air pockets.

Fig. 3 highlights a 3D XRCT reconstruction (Fig. 3a) and a single representative 2D cross-section (Fig. 3b) of a segment of an implant containing a crystalline small-molecule drug in a semi-crystalline polymer. In accord with studies varying the drug loading in the formulation (refer to section Drug Loading and Polymer Type), the brighter contrast features are identified as drug domains and the darker regions correspond to the polymer matrix. From the imaging

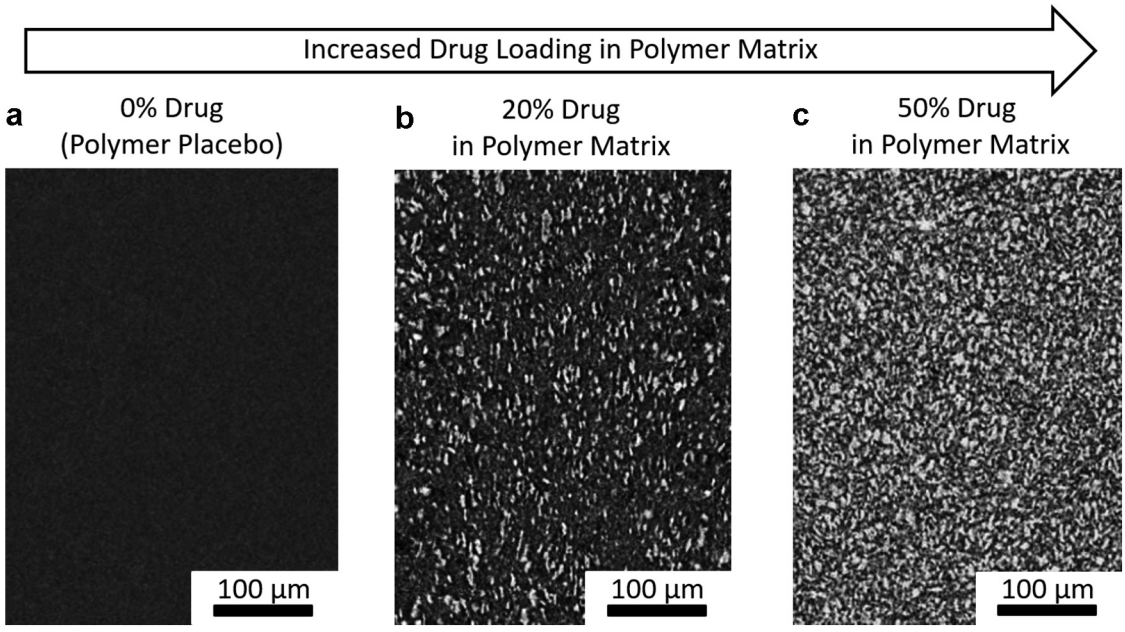

Fig. 7. X-ray CT 2D cross-sections of a matrix implants composed of a solid-dispersion of crystalline drug in a polymer matrix with varying drug loadings. (a) polymer placebo (0% drug). (b) 20% drug. (c) 50% drug.

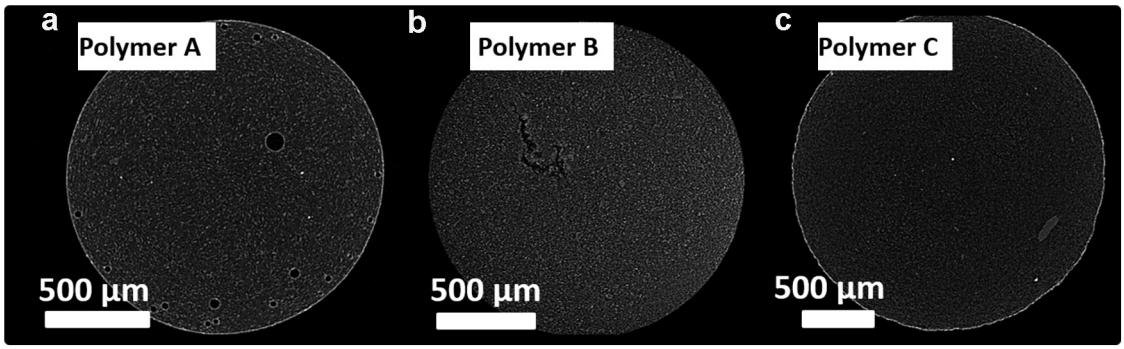

Fig. 8. X-ray CT images of implants manufactured from three different polymers. (a) PCL. (b) PLA. (c) EVA. (a) and (b) are biodegradable, but (c) is a non-biodegradable polymer.

it is confirmed that the drug domains in the polymer are regionally distributed in a relatively uniform manner throughout the implant. Furthermore, large agglomerates exceeding 30 µm in size are not observed. Micro-porosity in the implant is minimal (<0.3%). It is also apparent that the drug domains have some degree of mild preferred alignment, being oriented in a circular pattern in accord with directionality imparted by the fabrication method.

In addition to demonstrating the micro-domain structure in 2D, it is also possible to plot the drug distribution in 3D as shown in Fig. 4. The polymer has been digitally omitted from the representation by utilizing a simple software algorithm based on contrast segmentation. The white material is representing the 3D drug structure which can be used to study the spatial distribution and inter-domain connectivity (as will be discussed more in section Stages of Drug Release).

Micro-imaging can also be utilized to study micro-scale defects. Fig. 5 shows examples of small micro-cavities and drug agglomerates. As with large cavities, the micro-cavities appear as dark spots (low density regions) in the CT images. The pores shown range from 100 to 200 µm (Fig. 5a) to a few microns in size (Fig. 5b). Drug agglomerates, on the other hand, appear as sizable bright "islands" in the formulation (Fig. 5c). In this case, the agglomerates are attributed to drug due to the intrinsic contrast difference of drug/polymer and the absence of additional excipients in that particular formulation. The contrast between drug and polymer is discussed in more detail in section Drug Loading and Polymer Type and identification of features in complex multi-component compositions by chemical mapping is discussed in section Other Excipients and Chemical Mapping. The various defects can potentially impact formulation and quality control aspects in different ways. Metals can also be observed when introduced purposefully into the formulation as excipients, as discussed in section Other Excipients and Chemical Mapping.

Nano-Scale Structure

In the prior sections, micro-imaging has been shown to afford several applications towards the study of implant formulations. XRCT is a particularly convenient method due to its applications as a multi-scale imaging tool able to examine both the macro-scale (device-level) as well as the micro-scale (drug domain-level). However, a number of characteristics of implants can only be understood by detailed investigations of their nano-structure. In solid-dispersions, due to their limited resolution, micro-imaging methods are unable to resolve individual drug particles if the drug particle sizes are small (less than a few microns). On the other hand, nano-imaging techniques can resolve such small features. Furthermore, as we demonstrate, nano-imaging provides detailed information about the interface of the drug and polymer. We can infer information about the drug and polymer mixing by examining the encapsulation of the drug particles inside the solid dispersion.

In Fig. 6 nano-scale SEM and solid-state NMR are shown of a solid-dispersion composed of crystalline drug particles in a polymer matrix. The SEM secondary electron image in Fig. 6a resolves individual crystalline drug domains with high resolution, which appear as sharp-edged rectangular particles embedded in mold of polymer material (use of backscatter electron imaging could further improve the contrast between drug and polymer). While the drug domains are partly covered by polymer, there are many nano-separations

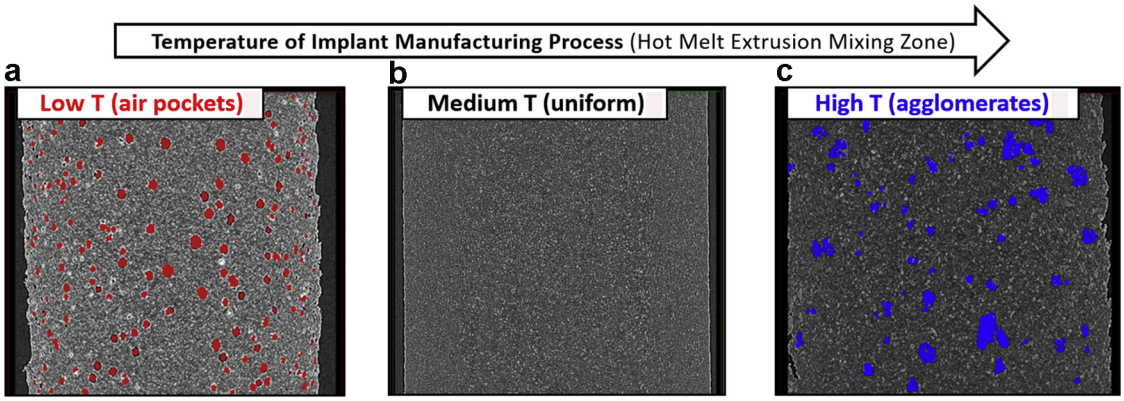

Fig. 9. X-ray CT images of matrix implants manufactured using different temperatures during hot melt extrusion. (a) Low-temperature manufacturing condition indicating air pockets that form (red circles). (b) Medium-temperature manufacturing condition indicating a uniform implant. (c) High-temperature manufacturing condition indicating sizable agglomerates (blue circles). Major defects were absent in the implant show in panel (b). The image dimensions are 2 × 2 mm.

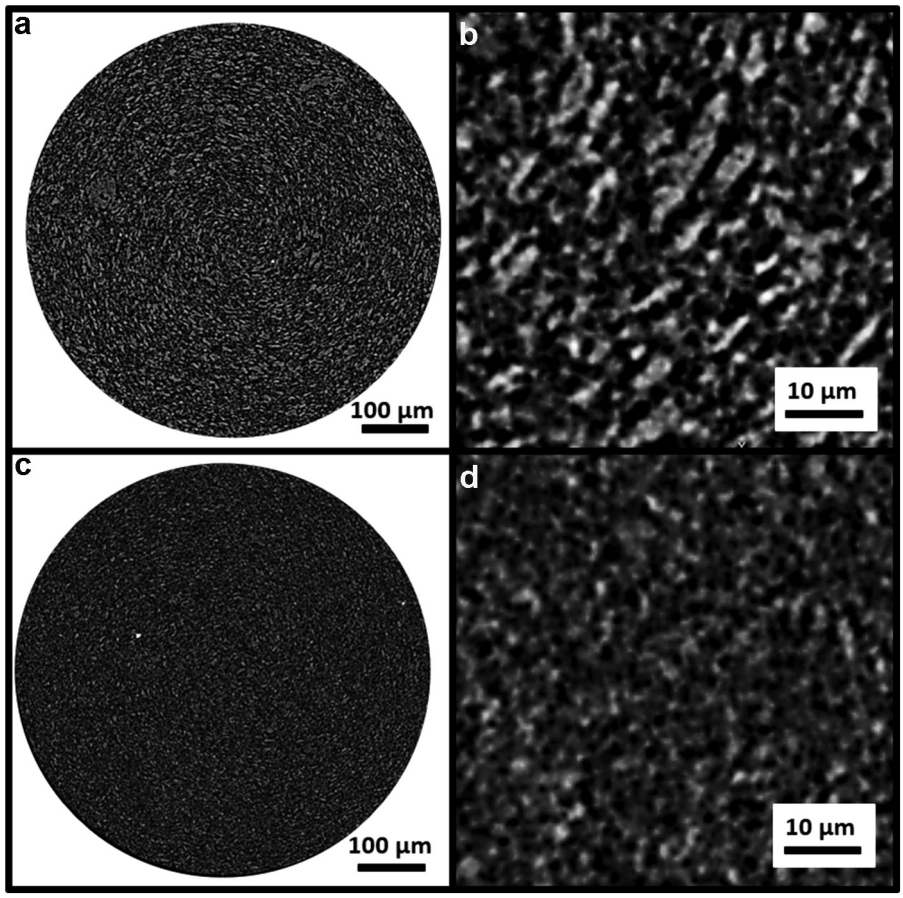

Fig. 10. X-ray CT images of matrix solid-dispersion implants produced under different shear force conditions. (a,b) Low-shear. (c,d) High-shear.

between the drug and polymer regions indicating that drug domains are not perfectly coated by the polymer. The image paints a qualitative picture that the system studied is predominantly phase separated. Indeed, solid-state NMR is used as a complementary spectroscopic tool to evaluate the extent of drug/polymer mixing by evaluating the crystalline-to-amorphous conversion. Fig. 6b shows the 13C CP-MAS spectra of the implant sample of interest, reference sample composed of 100% amorphous drug, as well as physical mixtures of crystalline API and polymer with 0%, 8%, and 15% amorphous contents spiked in. The spectral comparison evidences that this system has less than 8% amorphous content, corroborating the effective phase separation between crystalline drug and polymer that is suggested by the SEM data.

Formulation Composition Selection and Process Parameter Optimization

Having established imaging as a toolkit for analysis of pharmaceutical implants, a few case studies are highlighted examining specific variations to the formulation, *e.g.*, drug loading, excipient type, and manufacturing process conditions, and influence on implant structure.

Drug Loading and Polymer Type

Imaging can be utilized to evaluate the impact of variations in drug loading and polymer type on the formulation. In Fig. 7 multiple formulations are examined by XRCT varying the content of drug in the formulation. In the polymer placebo (Fig. 7a) there is a relative uniform background signal. With addition of 20% drug (Fig. 7b) individual drug domains appear with bright contrast relative to the background. As drug loading is further increased to 50% (Fig. 7c) the abundance of the drug domains correspondingly increases. (It is noted that drug loadings estimated from images are calculated on a *by-volume* basis, as compared to the values for drug loading that are keyed into the formulation fabrication process on a *by-weight* basis. The drug loadings on a volume percentage basis depend on the density of the materials. For the crystalline, small molecule pharmaceutical compounds studied here, the volume percentages are significantly lower than the drug loadings on a weight percentage basis.) This trend in contrast aligns intuitively with theoretically expected trends, as XRCT provides higher contrast for physically dense materials (such as crystalline drugs versus polymers containing amorphous regions) and those materials containing high atomic number species (such as halogens often found in pharmaceutical drugs). The inherent image contrast between drug and polymer can be used to study the impact of drug loading on the drug spatial distribution. The effect of drug loading variations from CT imaging can also be related directly to the drug release mechanism of the implants (as will be discussed in section Stages of Drug Release).

The impact of different polymer moieties on the implant structure can also be examined. Different polymer materials impact the manufacturing process, formulation, and performance in numerous ways. For example, different polymers can have varying degrees of miscibility with the drug. From a manufacturing standpoint, the process conditions and physicochemical properties of the resultant formulations are also impacted. In Fig. 8, implants are shown manufactured from three different polymer moieties: Polymer A (PCL) and Polymer B (PLA) are two biodegradable and amorphous polymers. Polymer C (EVA) is a non-degradable and

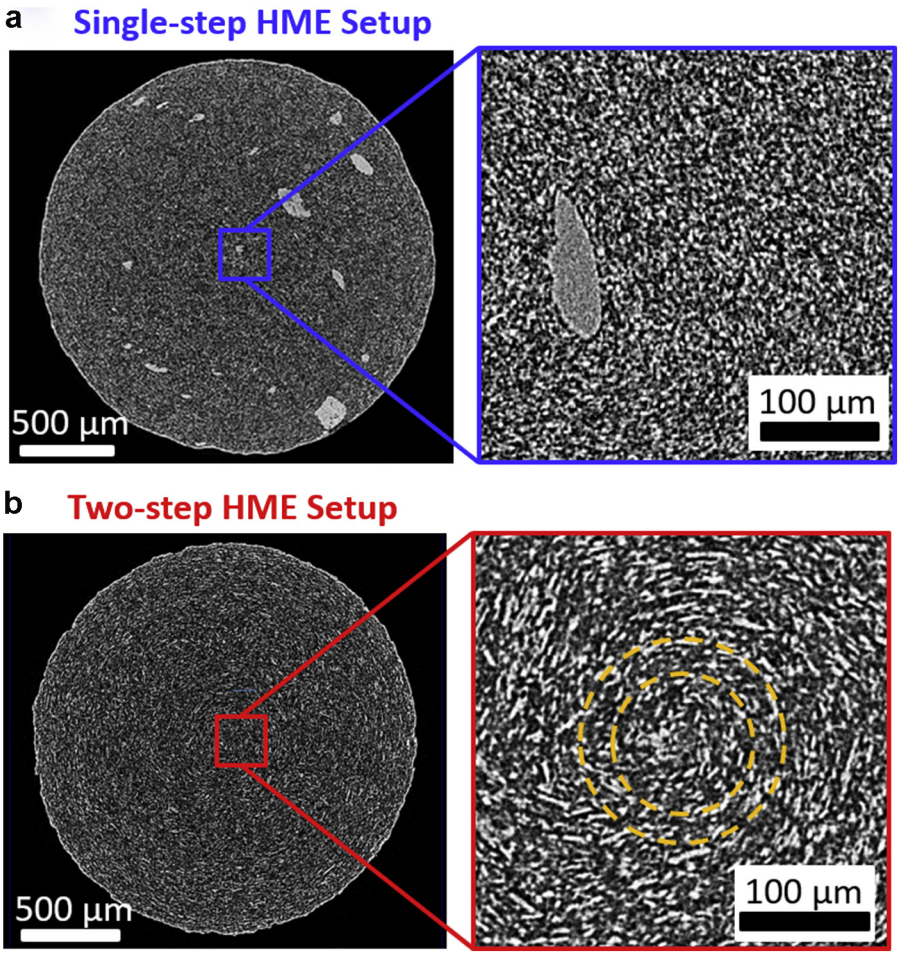

Fig. 11. X-ray CT 2D cross-sections comparing two formulations produced by different hot melt extrusion setups. (a) Single-step extrusion setup. (b) Two-step extrusion setup.

semi-crystalline polymer. The drug is identical in all three cases (crystalline small molecule). The preferred extrusion temperatures increased across the series from A - > B - > C (75 °C -> 100 °C -> 125 °C). In all three cases, drug domains (bright dots) are resolved as distinct features embedded in the matrix (note that the instrument conducted an auto-calibration of overall intensity between the datasets to optimize image quality; hence the intrinsic contrast difference between Polymer A vs B vs C across the data sets may not necessarily be solely due to differences in material properties). The data is consistent with an understanding obtained from other physical characterization methods (*e.g.*, X-ray diffraction and ssNMR) that the physical state of the high-melt drug crystals is relatively stable during the manufacturing process and drug/polymer mixing is minimal. Thus, the data speaks to the feasibility of all three polymer moieties towards generating structurally uniform implants by a holt melt extrusion process. However, it is noted that Polymer A (extruded at the lowest temperature) exhibits the highest porosity and Polymer C (extruded at the highest

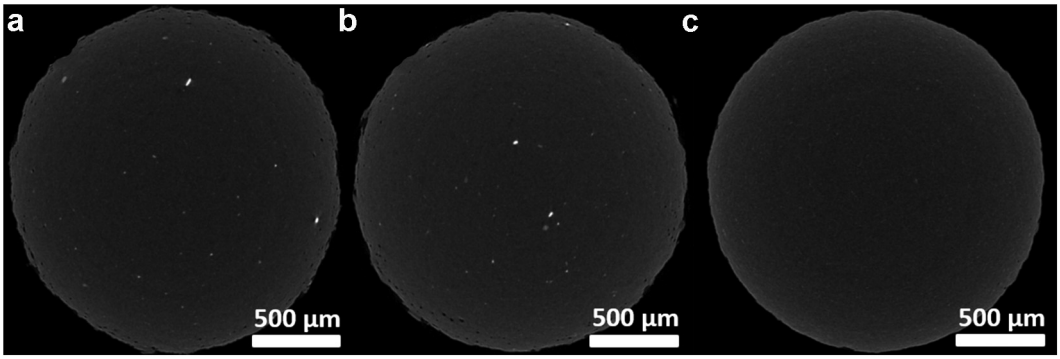

Fig. 12. X-ray CT images of implants containing drug, polymer, and a metal sulfate ($BaSO_4$). Formulations were made with different process conditions examining the dispersion of the metal in the formulation. (a) Co-mill polymer and $BaSO_4$. (b) Similar as in (a) but with addition of a simple shear extrusion screen pack. (c) Alternative screw design with additional kneading blocks.

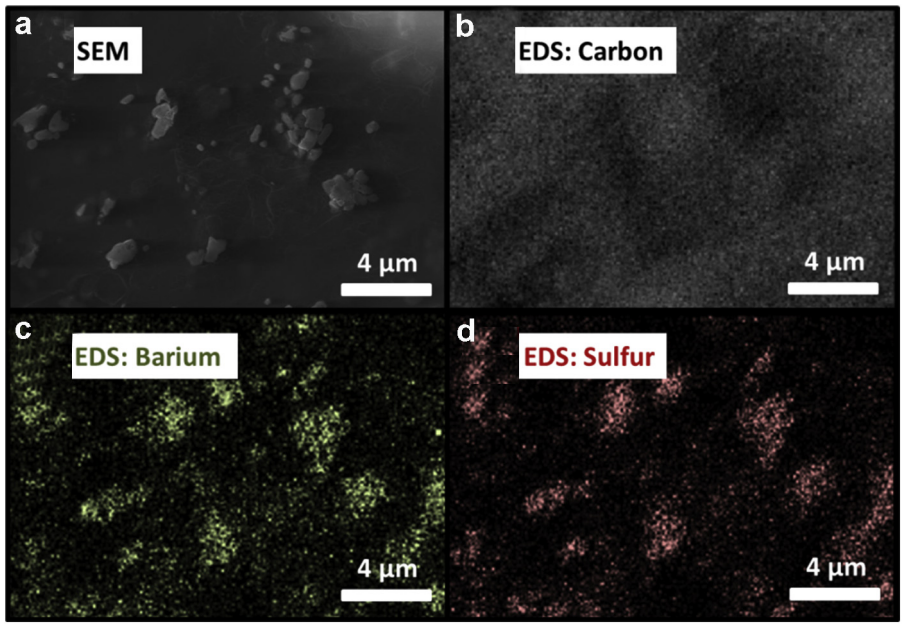

Fig. 13. Energy-dispersive X-ray spectroscopy (EDS) SEM imaging of a matrix solid-dispersion formulation composed of drug, polymer, and a radiopaque agent (barium sulfate). (a) SEM image. (b) Carbon EDS. (c) Barium EDS. (d) Sulfur EDS.

temperatures) exhibits the lowest porosity. Further, it is of note that the nature of the porosity is different for Polymer A (total micro-porosity *ca.* 1%; spherical cavities) and Polymer B (total micropo-rosity *ca.* 0.5%; elongated crack-like cavities; refer to the supporting information). This data proved to be a key input informing process development studies and adapting the process to give the preferred outputs. The temperatures and process conditions used for two of the polymers A and B were inadequate and were needing to be adjusted to account for the different inherent properties of the polymers. The effect of temperature on the porosity of HME-manufactured implants is further discussed in the next section.

Process Conditions (HME Setup, Temperature, Shear Force)

After key implant formulation aspects are solidified (overall formulation design, manufacturing method, composition), important questions in mid- and late-stage development are centered around defining the range of manufacturing process parameters which yield comparable drug release performance within defined specifications. Problematically, for long-acting formulations acquiring *in-vitro* and *in-vivo* drug release profiles for all tested formulations is extremely time-consuming. Imaging can be leveraged as a screening tool to select the most promising formulation candidates for further release testing.

The first example of utilizing imaging to inform process engineers and scientists on process parameter selection is a variation in the processing temperature for hot melt extrusion (Fig. 9). Within a fixed formulation composition (same polymer and same drug loading), a clear difference in macro-scale uniformity is observed as a function of temperature. Lower temperature extrusions (Fig. 9a) yield formulations with a significant proportion of defects in the form of air cavities (shown by the red dots). At those low temperatures the polymer viscosity is still rather high which hinders the filling of air pockets during the HME manufacture. On the other hand, at high temperatures (Fig. 9c) porosity is minimal but there is an increased propensity towards drug agglomeration (shown by the blue dots). The optimal formulation structural uniformity was attained in the intermediate range (Fig. 9b).

The second example demonstrates the effect of shear forces during the manufacturing process on the implant micro-structure. In Fig. 10 an example is shown comparing lower shear forces

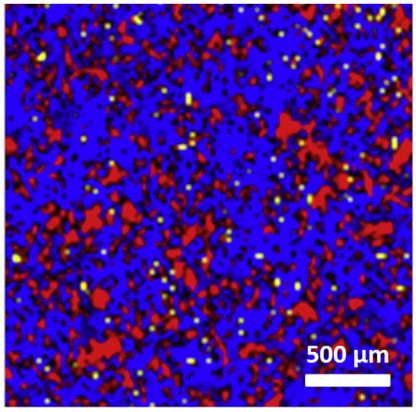

Component	Target Concentration (%wt)	Image Component Analysis
Drug	40%	36.4%
Barium Sulfate	10%	7.3%
Polymer	50%	56.3%

Fig. 14. Raman mapping data of a matrix solid-dispersion implant composed of 40% drug, 10% barium sulfate, and 50% polymer by weight. The image component analysis was conducted on a by-volume basis.

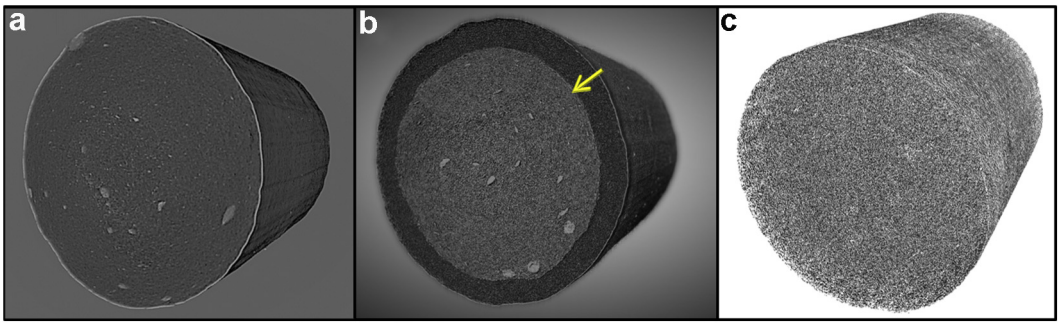

Fig. 15. Complete 3D representation of matrix solid dispersion implants after different stages of drug release. (a) Implant as-fabricated prior to undergoing the release process. (b) Implant that has undergone 18% drug release shows a dissolution front, indicated by the yellow arrow, penetrating into the interior of the implant. (c) After 100% drug release, only the porous husk of the polymer remains behind. In this case the polymer is non-biodegradable. The implant rods have a cylindrical diameter of 2 mm.

(Fig. 10a) versus higher shear forces (Fig. 10b). The differences between the shear conditions are explained in the experimental section. The effect of shear rate was found to be significant on the microdomain structure. The higher shear forces significantly decreased drug agglomeration. The high-shear manufacturing condition yielded for the implant an approximately two-fold increased release rate as compared to the implant manufactured under low-shear manufacturing conditions.

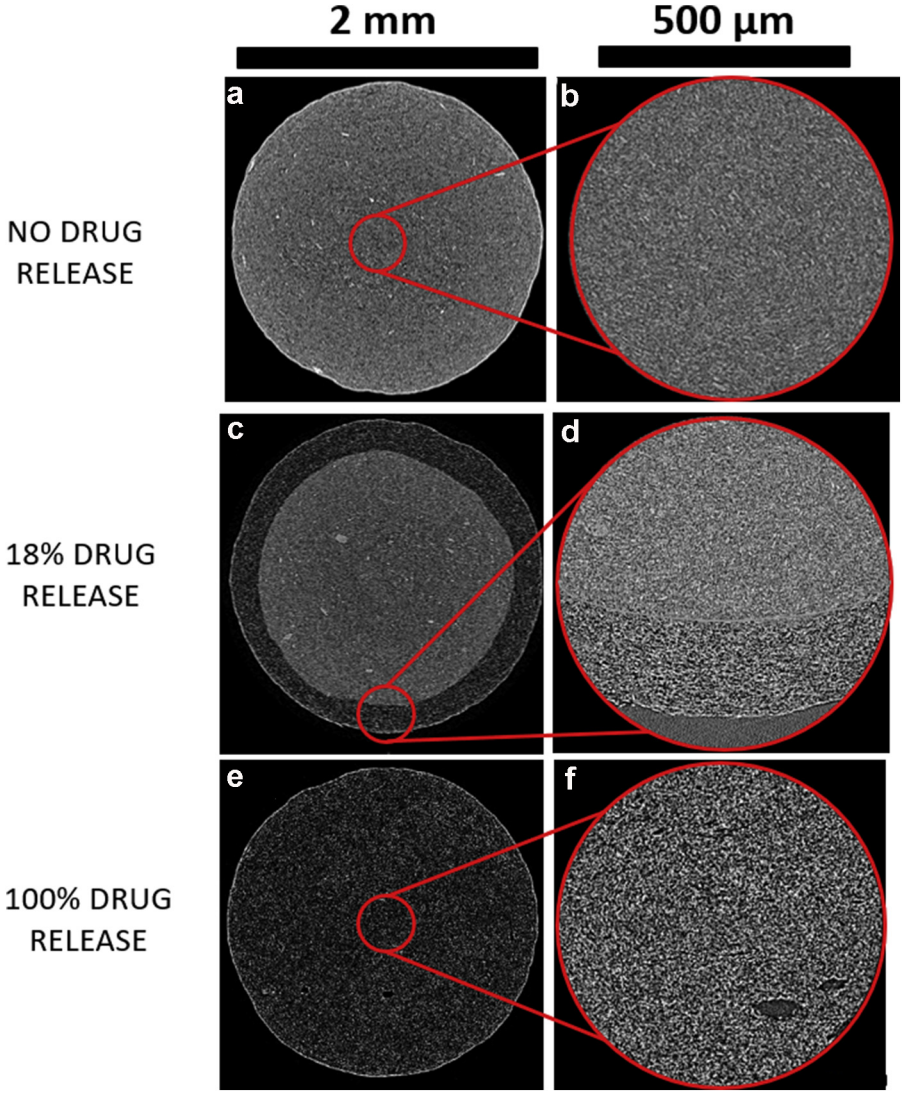

Fig. 16. X-ray CT images 2D cross-sections and high magnification images of a matrix solid dispersion implants at different stages of release. (a,b) As-fabricated; *i.e.*, at the initial pre-release state. (c,d) After 18% of drug has released. (e,f) After 100% of drug has released. The released implants were imaged after removal from the dissolution bath. The image dimensions are 2 × 2 mm.

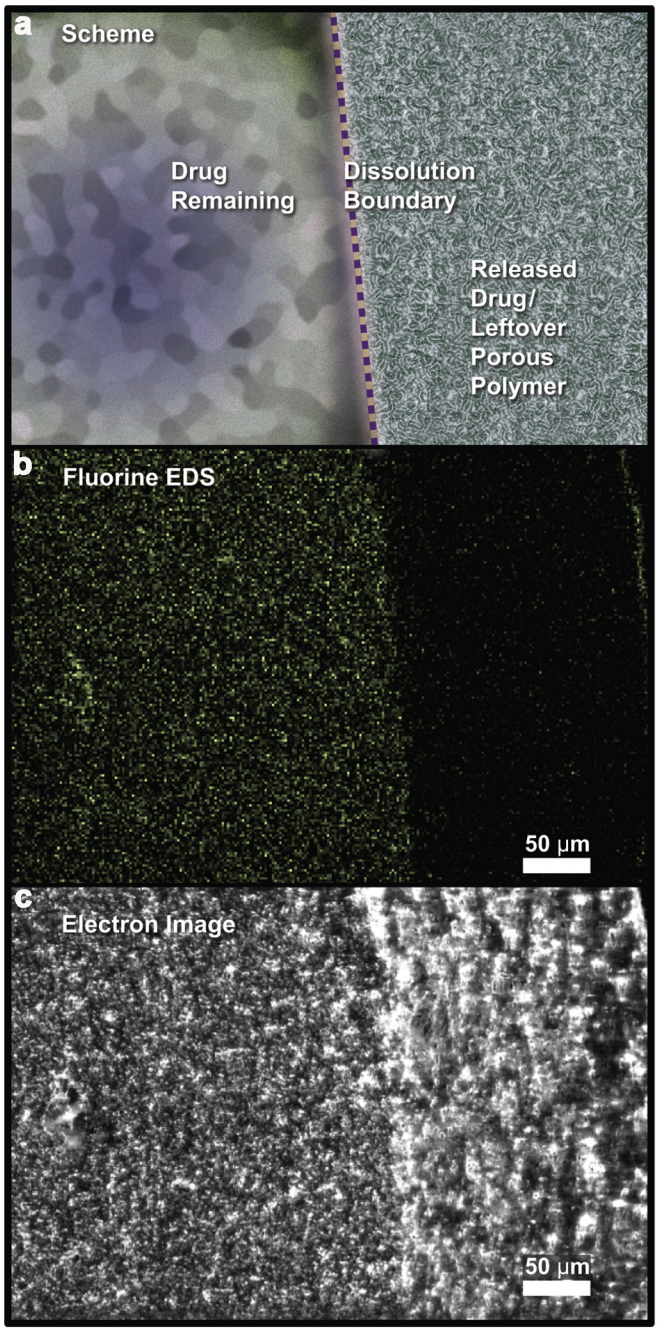

Fig. 17. Chemical evidence for drug dissolution from EDS. (a) Scheme of the dissolution front between regions where drug remains and regions where drug has been released. (b) Corresponding to the scheme in (a), EDS mapping data of the fluorine signal (green) which is a unique signature of the drug in this system. (c) Corresponding electron image.

A third example demonstrates a more drastic variation in hot melt extrusion setup (Fig. 11). In Fig. 11a a single-step extrusion was performed, wherein a preblend was directly fed through a small twin screw extruder. In Fig. 11b a two-step extrusion was performed, where a preblend was fed thru a twin-screw extruder, pelletized, and then fed through a single-screw extruder. These two conditions impart different shear forces, heat history, and orientational effects. These differences can be picked up as variations in the drug microstructure. In Fig. 11a various large agglomerates >30 μm in size are observed, which appear as white islands in the implant. (The islands appear to have a bright skin/boundary which is likely due to operating under conditions favorable for X-ray phase contrast, which affords additional contrast at the edges/boundaries of materials.) These large islands are absent in Fig. 11b. However, aside from the large islands, other drug domain features are overall larger in Fig. 11b. Furthermore, in Fig. 11b the drug domains are radially oriented in the sample. The average size of agglomerate domains in the low-shear case was ca. 30 μm, whereas agglomerate domains were smaller in the high-shear case at ca. 15 μm. The microstructural differences significantly impacted the release rate. The single-step HME setup yielded for the implant an approximately two-fold increased release rate as compared to the implant manufactured from the two-step HME setup.

Other Excipients and Chemical mapping

Thus far, solid-dispersion matrix implants have been examined that contained only two components: the active drug to achieve the targeted therapeutic effect as well as the polymer to produce a solid implant and slow the release rate. However, it is often desirable to include in the formulation additional excipients. For example, heavy metals may be utilized as a radiopaque agents for *in-vivo* imaging of implants, as well as other excipients which may enhance the formulation process in various ways.

Imaging techniques can help understand the impact of additional components on the formulation uniformity. In Fig. 12, a heavy metal ($BaSO_4$) is incorporated along with drug/polymer and the degree of metal agglomeration/dispersion is studied under the influence of different process conditions. In the XRCT images the metal appears vibrantly bright and dotted throughout the formulation. It is shown that some processes are better with respect to dispersing the metal effectively to achieve a uniform microdistribution and reducing formation of large agglomerate clusters. In Fig. 12a, $BaSO_4$ was blended with polymer and then subsequently milled, with the intent to utilize shear from the milling process to aid in the dispersion. In Fig. 12b, a similar process was used, but with addition of simple shear extrusion screen pack to break apart large agglomerates. The imaging results demonstrate that agglomerates of $BaSO_4$ were present under both processing conditions in Fig. 12a and b. On the other hand, in Fig. 12c additional kneading blocks in the mixing section were used to achieve more aggressive shear. Thus, kneading blocks appear to have eliminated large $BaSO_4$ aggregates.

As has been shown, imaging techniques like XRCT can resolve structural differences between components in an implant. However, reliable chemical differentiation of individual constituents in many-component systems is challenging and requires methods with higher chemical sensitivity. For this purpose, elemental and chemical mapping methods are of interest. One example of elemental mapping is EDS-SEM which can resolve the spatial distribution of elements in a material and can be applied to implants. Elemental mapping is important when different substituent components in an implant cannot easily be distinguished based on structural attributes; *e.g.*, for formulation components that have similar particle sizes and morphologies. Elemental mapping can be applied to both drugs as well as excipients. Small molecule drugs frequently contain halogens that are drug-specific. The tracing of drug after dissolution by elemental API-specific halogen mapping is discussed in section Stages of Drug Release (see Fig. 17). As discussed previously, many pharmaceutical formulations also contain metals that can be identified with elemental mapping. Fig. 13 shows nano-scale SEM-EDS images of a local region in a matrix solid-dispersion implant containing drug, polymer, and $BaSO_4$. In the SEM image in Fig. 13a numerous particles are resolved that are a few microns in size. Corresponding EDS information is provided for carbon (Fig. 13b), barium (Fig. 13c), and sulfur (Fig. 13d), identifying

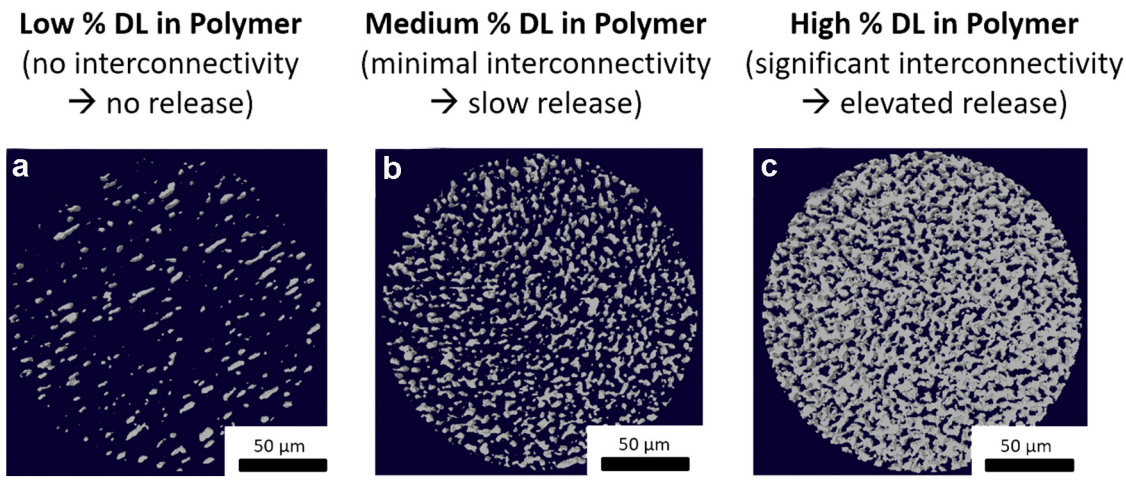

Fig. 18. X-ray CT images of implants manufactured using different drug loadings. A representative sub-volume of the whole implant is shown. Drug domain connectivity is shown in white/gray. The polymer is digitally omitted. Each image is a representation of 30 2D slices, which construct a volume of 21 μm thickness. (a) Drug loading below the percolation threshold. (b) Drug loading slightly above the percolation threshold. (c) Drug loading significantly above the percolation threshold.

the domains as barium sulfate. Elemental mapping enables the identification of excipient domains and can help understand their structure and spatial distribution in the formulation, in a more unambiguous assessment than is possible with less chemically sensitive imaging methods.

Another example of chemically-sensitive mapping for implant applications is Raman imaging, which can be used to distinguish regions of drug, polymer, and other excipients by taking advantage of the high chemical sensitivity of Raman spectroscopy. In its ability to resolve subtle differences in the chemical state beyond merely elemental differences, Raman is an even more powerful tool for spatiochemical mapping. In Fig. 14 an implant composed of drug, polymer, and barium sulfate is shown. The chemical distribution of the materials is visualized and the volume factions of each component are computed from image analysis.

Stages of Drug Release

Another advantage of imaging is that it can help understand the drug release process from implants. Imaging can be used to understand the mechanism by which drug diffuses through the implant and to confirm that release is occurring in an expected way. It is noted that the investigation of implant drug release by *in-vivo* imaging is beyond the scope of this work, being rather focused on the effect that dissolution has on the formulation material itself. Also, a detailed model for the drug release and its correlation to CT micro-imaging data is presented in a separate publication.[22]

Fig. 15 shows 3D XRCT reconstructions of implants after different stages of drug release. In Fig. 15a the implant has undergone partial release. A dissolution front has penetrated into the implant from the surface exposed to the dissolution medium, as indicated by the yellow arrow. In Fig. 15b an implant is shown after complete release. The porous polymer husk is left behind after the drug has completely diffused out of the implant into the dissolution medium (the polymer in this case is non-biodegradable, which is confirmed by imaging of the porous polymer matrix that remains after complete drug release). A detailed look at the microstructure, in 2D cross-sections with two different magnification levels (4× and 20×), is provided in Fig. 16. In Fig. 16a and b the implant is shown as-fabricated (prior to dissolution). In Fig. 16c and d the implant is shown after 18% of the drug has released with the dissolution boundary being readily apparent. In Fig. 16e and f the implant is shown after complete release.

In comparison to traditional dissolution studies, which examine the total amount of drug release over time, spatially-resolved imaging is helpful to verify that the drug release from the implants is occurring in a structurally uniform manner. The dissolution front is shown to be progressing though the implant equally and uniformly from the circular perimeter of the implant. This type of analysis can help diagnose unexplained behaviors that may be observed in dissolution studies if release is structurally non-uniform.

Chemical mapping can also be utilized to confirm release of the drug. In Fig. 17 EDS mapping of fluorine, an element specific to the drug, is shown of a partially-release implant along with a corresponding cartoon representation. The image shows a case that is similar to the partially released implant in Fig. 16c–d, but zoomed-in at the dissolving boundary with higher resolution electron microscopy and added elemental mapping capability. The image looks at the dissolution front separating the region where drug had already released (the right side of the image) and the region where the drug remains (the left side of the image). The region from which drug was postulated to have been released was indeed depleted of the drug-specific fluorine signal. EDS mapping provides compelling *chemical* evidence that the drug release from the implant can be monitored by imaging, corroborating the observations made by the chemically less sensitive CT method in Figs. 15 and 16, and confirms that there is uniform release.

Finally, quantitative imaging can also be applied to explain the mechanism of drug release. Fig. 18 shows XRCT images of different % drug loadings in a matrix solid dispersion formulation. The formulation is a bi-component implant composed of drug and polymer. In the experimental dissolution data it was found that drug release does not increase linearly with drug loading. The drug in this case has negligible diffusivity through the polymer material and the polymer is non-degradable. It was hypothesized that this non-linear correlation of drug loading and release was due to the increase in long-range connectivity in the formulation. At low drug loadings many drug domains are surrounded by polymer and those drug domains are not accessible towards the dissolution medium. As drug loading is increased, drug interconnectivity also correspondingly increases resulting in channels for release. XRCT was leveraged to provide experimental evidence for this hypothesis. In the images, the entire implant is not shown, rather to reduce visual clutter only a sub-volume of the whole implant structure is analyzed. Furthermore, the polymer is omitted and only the drug domains are presented (gray features). These sub-volume

representations allow visualization of the local drug domain interconnectivity. The images demonstrate that domain interconnectivity tracked qualitatively with increased drug loading in a manner that is sensible when contrasted against the non-linear release trends. We note that these phenomena are not new and are well-known theoretically for the formation of long-range connectivity in random systems. The novelty lies in the ability to visually illustrate this effect by direct experimental observation through imaging.

Conclusions

Materials imaging methodologies are demonstrated to possess a multitude of applications towards long-acting polymeric implants. These tools can inform at different stages of pharmaceutical development on formulation selection, process optimization, batch consistency, as well as acquiring a detailed understanding of the drug release mechanism. As a non-destructive and multi-purpose 3D method, X-ray computed tomography has broad utility to interrogate key physical attributes of solid implants for quality control and to evaluate the impact of manufacturing processes on the microstructure and release performance. XRCT is an excellent method to gain insights into solid pharmaceutical implant development both during early formulation screening as well as later-stage process robustness studies. The limitations of X-ray imaging, specifically the lower resolution and limited chemical specificity, are overcome by use of complementary scanning electron microscopy and Raman microscopy tools which provide further insight into nanoscale and chemical aspects. Materials imaging holds promise for continued expansion in the pharmaceutical industry with an ever-increasing push towards alternative and novel drug delivery modalities.

Appendix A. Supplementary Data

Supplementary data to this article can be found online at https://doi.org/10.1016/j.xphs.2020.05.031.

References

1. Maniruzzaman M, Boateng JS, Snowden MJ, Douroumis D. A review of hot-melt extrusion: process technology to pharmaceutical products. *ISRN Pharm*. 2012;2012:436763.
2. Baghel S, Cathcart H, O'Reilly NJ. Polymeric amorphous solid dispersions: a review of amorphization, crystallization, stabilization, solid-state characterization, and aqueous solubilization of biopharmaceutical classification system class II drugs. *J Pharm Sci*. 2016;105(9):2527-2544.
3. Musiime S, Muhairwe F, Rutagengwa A, et al. Adherence to highly active antiretroviral treatment in HIV-infected Rwandan women. *PLoS One*. 2011;6(11):e27832.
4. Ramirez Garcia P, Cote JK. Factors affecting adherence to antiretroviral therapy in people living with HIV/AIDS. *J Assoc Nurses AIDS Care*. 2003;14(4):37-45.
5. Whetten K, Reif S, Whetten R, Murphy-McMillan LK. Trauma, mental health, distrust, and stigma among HIV-Positive persons: implications for effective care. *Psychosom Med*. 2008;70(5):531-538.
6. Barrett SE, Teller RS, Forster SP, et al. Extended-duration MK-8591-eluting implant as a candidate for HIV treatment and prevention. *Antimicrobial Agents Chemother*. 2018;62(10):e01058.
7. Campbell BR, Gonzalez Trotter D, Hines CDG, et al. In vivo imaging in pharmaceutical development and its impact on the 3Rs. *ILAR J*. 2016;57(2):212-220.
8. Swales JG, Hamm G, Clench MR, Goodwin RJA. Mass spectrometry imaging and its application in pharmaceutical research and development: a concise review. *Int J Mass Spectrom*. 2019;437:99-112.
9. Tian Z, Bing NC, Xie LI, Wang LJ, Yuan H. *2011 Third International Conference on Measuring Technology and Mechatronics Automation*. vols. 6–7. 2011:943-947.
10. Kempson IM, Prestidge CA. Mass spectrometry imaging of pharmaceuticals: from tablets to tissues. In: Müllertz A, Perrie Y, Rades T, eds. *Analytical Techniques in the Pharmaceutical Sciences*. New York, NY: Springer New York; 2016:629-647.
11. Seitavuopio P, Rantanen J, Yliruusi J. Tablet surface characterisation by various imaging techniques. *Int J Pharm*. 2003;254(2):281-286.
12. Buckwalter KA, Parr JA, Choplin RH, Capello WN. Multichannel CT imaging of orthopedic hardware and implants. *Semin Musculoskelet Radiol*. 2006;10(1):86-97.
13. Bourges JL, Bloquel C, Thomas A, et al. Intraocular implants for extended drug delivery: therapeutic applications. *Adv Drug Deliv Rev*. 2006;58(11):1182-1202.
14. Kreye F, Hamm G, Karrout Y, et al. MALDI-TOF MS imaging of controlled release implants. *J Control Release*. 2012;161(1):98-108.
15. Beyer S, Xie L, Schmidt M, et al. Optimizing novel implant formulations for the prolonged release of biopharmaceuticals using in vitro and in vivo imaging techniques. *J Control Release*. 2016;235:352-364.
16. Stankovic M, Frijlink HW, Hinrichs WLJ. Polymeric formulations for drug release prepared by hot melt extrusion: application and characterization. *Drug Discov Today*. 2015;20(7):812-823.
17. Otsu N. Threshold selection method from gray-level histograms. *IEEE Trans Syst Man Cybern*. 1979;9(1):62-66.
18. Stewart S, Priore RJ, Nelson MP, Treado PJ. Raman imaging. *Annu Rev Anal Chem*. 2012;5:337-360.
19. Zhang XC, Wyss UP, Pichora D, Amsden B, Goosen MFA. Controlled-release of albumin from biodegradable poly(Dl-lactide) cylinders. *J Control Release*. 1993;25(1-2):61-69.
20. Zhou TH, Lewis H, Foster RE, Schwendeman SP. Development of a multiple-drug delivery implant for intraocular management of proliferative vitreoretinopathy. *J Control Release*. 1998;55(2-3):281-295.
21. Zhu GZ, Mallery SR, Schwendeman SP. Stabilization of proteins encapsulated in injectable poly (lactide-co-glycolide). *Nat Biotechnol*. 2000;18(1):52-57.
22. Irizarry R, Skomski D, Chen A, et al. Theoretical modeling and mechanism of drug release from long-acting parenteral implants by microstructural image characterization. *Ind Eng Chem Res*. 2018;57(45):15329-15345.